"AL. I CUZA" UNIVERSITY OF IASSY
FACULTY OF PHYSICS

Contributions to the study of nanoparticle systems used in magnetic hyperthermia

-Summary-

SCIENTIFIC COORDINATOR:
Prof. Univ. Dr. Ovidiu Florin CĂLȚUN

Ph.D STUDENT:
Anamaria DOAGĂ

IASSY, September 2013

For the attention of

.....

"AL. I CUZA" UNIVERSITY OF IASSY

We inform you that on the 26th September 2013, at 14ooh in the room L1, doctoral candidate Anamaria Doaga will present in open meeting her doctor degree dissertation entitled

"Contributions to the study of nanoparticle systems used in the magnetic hyperthermia"

with the view to obtain the scientific PhD title of PhD.

The **Doctoral Commission** consists of:

Chairman:

PhD Prof. Diana Mardare, Faculty of Physics, „Al. I. Cuza" University of Iassy

Scientific Coordinator:

PhD Prof. Ovidiu-Florin Călțun, Faculty of Physics, „Al. I. Cuza" University of Iassy

Referents:

PhD Prof. Mircea- Niculae Palamaru, Faculty of Chemistry**,** "Al.I. Cuza" University of Iassy

PhD Prof. Simion Simon, Faculty of Physics, "Babes Bolyai" University of Cluj-Napoca

PhD. Prof. Rolf Hempelmann, Physikalische Chemie, Universität des Saarlandes, Saarbrucken, Germany

Thanks

On the occasion of finishing my dissertation, I want to express my deep respect and appreciation for the scientific coordinator, PhD. Professor Ovidiu Florin Caltun, who contributed to my professional formation. I want to thank him for his support; his pieces of advice always arrived at the right moment, and for his patience and confidence all along these years.

With special consideration and respect, I address my thanks to the members of the Referent Commission, PhD Prof. Mircea-Niculae Palamaru, PhD Prof. Simion Simon and PhD Prof. Rolf Hempelmann, who kindly analyzed and evaluated the scientific objectives presented in this dissertation.

I thank to the Guidance Commission, PhD Prof. Alexandru Stancu, PhD Prof. Lect. Ioan Dumitriu and PhD Prof. Lect. Iordana Astefanoaiei for their encouragement, precious suggestions and support offered in my scientific activity.

I thank to PhD Prof. Rolf Hempelmann and the team from the Laboratory from the Physical Chemistry Department of the University of Saarland, Germany, for their co-operation and support.

I thank the laboratory team, together with who I started to make my first steps in the world of research.

This work was supported by the European Social Fund in Romania, under the responsibility of the Managing Authority for the Sectoral Operational Programme for Human Resources Development 2007-2013 [grant POSDRU/107/1.5/S/78342]. I also want to thank to the entire project team for the lent financial support.

Content

The summary of the doctoral dissertation preserves the numbering of chapters, figures, tables and literature indications.

INTRODUCTION

During the recent years there are major interests in the technologies of nanostructures materials. The magnetic nanomaterials offer several advantages due to their nanosize (≤ 100 nm), as well as to their unique structural and magnetic properties. Given the wide scale applications of the magnetic nanoparticles in biomedical field, biotechnology, engineering, materials science, etc, a great attention was paid to the preparation of various types of particles.

A nanoparticle category with wide applicability is represented by the nanoparticles with spinel structure, made of iron oxides, such as: magnetite Fe_3O_4, maghemite γ-Fe_2O, MFe_2O_4 (M= Mn, Mg, Ni, Co, Zn, etc). Their utilization in biomedical purposes, such as in imagery based on magnetic resonance (RMN) as contrast agents, in marking the cancer- affected tissues, in magnetic hyperthermia treatment, in magnetically controlled transport and release of medicamentary substances, brought a major contribution to the evolution of medical treatment and technology. The previous studies concerning the toxicity of iron oxides and of aqueous solutions based on metallic oxides have proved that these show the lowest toxicity.

The chosen research theme concerning the utilization of magnetic nanoparticles and of aqueous solutions based on metallic oxides in magnetic hyperthermia is quite present in the international research due to its biomedical applications.

This work is structured on two basic directions: the topicality and importance of the theme in the national and international research, and personal contributions in this research field. The thesis is divided in four chapters and ends with some general conclusions.

Chapter I
Introductory notions about magnetic hyperthermia

1.1. General notions

For medical application, especially important are the magnetic nanoparticles with ferromagnetic properties in the form MFe_2O_4, where M can be Mn, Co, Ni, Zn, etc. These nanoparticles

were synthesized through various methods in order to produce bio-compatible and stable particles with controlled shape, and to have a good dispersivity in surfactants. The mostly used methods for high quality magnetic nanoparticles synthesis include co-precipitation, thermal decomposition, hydrothermal synthesis and laser induced pyrolysis [1]. The co-precipitation is a convenient and easy method to synthesize iron oxides (Fe_3O_4 or γ-Fe_2O_3) from aqueous solutions through the addition of a base at room temperature or high temperatures. The shape and composition of these nanoparticles also depend on the type of utilized salts (chlorides, sulphates, nitrates, etc), on the pH value and on some reaction parameters, such as temperature and solution stirring rate during the synthesis [2].

1.2. Hyperthermia

The hyperthermia, heat treatment or thermotherapy is considered as one of the cancer therapies which, in combination with radiotherapy and chemotherapy lead to significant results in the treatment of several affections, cancer included. It is often difficult to aim exactly the specific cancer cells. Any attempt to destroy the tumor cells can result in the deterioration of the normal cells surrounding them. One of the advantages of the thermal treatment is that it permits to heat very small areas of the body, thus avoiding the deterioration of the tissues adjacent to the cancerous zone [3].

The hyperthermia is a natural or artificial phenomenon which implies increasing the temperature of the body or of a part of it above the temperature established at a certain moment by the organism thermo-regulatory system. The treatment is based on the fact that a temperature increase between 40^o and 48^oC for an hour or more induces the death of the tumor cells [4].

In order to obtain the maximum efficiency of the treatment, the magnetic hyperthermia uses nanoparticles with various chemical compositions which are introduced inside the affected tissue as sources for tumor tissue heating. The dimensions of the nanoparticles used for this goal must be smaller than 100 nm. The method implies placing the magnetic nanoparticles within an alternative magnetic field. The studies concerning the application of this treatment method are thoroughly focused on the nanoparticles properties, the methods to introduce them inside the organism, the heating techniques and temperature control in the tumor tissue [5].

1.3. Types of hyperthermia

Depending on the localization of the heat sources, the hyperthermia can be classified in external hyperthermia and internal hyperthermia. In the case of external hyperthermia, the heat transfer is performed from outside the body through various methods, such as microwaves, radiofrequency waves, ultrasounds, etc, while the internal hyperthermia is based on introducing the heat sources inside the body [6].

According to the heat transport technique, one can speak about local or regional hyperthermia or the hyperthermia of the entire body.

1.4. Types of nanoparticles used in hyperthermia

As far back as 1957 Gilchrist and Co [7] proposed the utilization of magnetic materials in hyperthermia. The particles used in hyperthermia present ferro- or ferri-magnetic properties. Pankhurst and Co. [8] reported that the magnetic particles present magnetic properties in the absence of the applied magnetic field. The magnetic particles used in hyperthermia possess magnetic moment and can have permanent magnetic orientations. At present, the dextran-covered magnetite, with a Curie temperature of 58.5^{o}C is widely used as hyperthermic agent [4].

1.4.1. Cobalt ferrite

The cobalt ferrite was also applied in hyperthermia by Pradhan and Co. [9] in 2005. They synthesized superparamagnetic nanoparticles of Fe_3O_4, $MnFe_2O_4$ and $CoFe_2O_4$ through co-precipitation in nitrogen atmosphere. The SAR value for cobalt (37 W/g) was smaller than for the manganese ferrite (120 W/g) and magnetite (97 W/g).

1.4.2. Magnetite and maghemite

The magnetic nanoparticles mostly studied in the hyperthermia process were magnetite and maghemite. Ma &Co. studied through calorimetric method the influence of magnetite nanoparticles size (7.5, 13, 46, 81, 282 and 416 nm) on the specific absorption rate (SAR), investigating the temperature dependence on the time while the magnetic field is applied (80 kHz, 32.5

kA/m)[10]. The author noticed that the SAR value for the magnetite nanoparticles strongly depend on nanoparticles size.

1.4.3. Manganese Ferrite

Unlike cobalt, the manganese is less toxic for the human organism, which justified the studies dedicated to the production of nanoparticles able to increase the temperature of the medium in which they are introduced even in small quantities. With this aim in view, studies were performed on manganese ferrite with applications in hyperthermia.

1.4.4. Zinc ferrite

Simultaneous studies were also carried out on the zinc ferrite with applications in hyperthermia.

1.5. Mechanisms of ferrofluids heating

The magnetization processes suffered by the magnetic nanoparticles depend on the amplitude and frequency of the applied magnetic field and can determine them and the medium in which they are dispersed to get heated. The energy losses characteristic to nanoparticles systems situated in an alternative magnetic field are of several types: the hysteresis losses, Néel and Brown relaxations and eddy current losses (Foucault currents).

1.5.1. Hysteresis losses

The hysteresis losses are directly proportional with the area of the hysteresis loop. These depend on the shape of the hysteresis loop, their diminution being determined by the utilization of certain materials with a narrow hysteresis loop. These losses come from the delay of the magnetic induction in the substance in following the fast variations of the magnetic field intensity between negative and positive fields. The area encircled by the hysteresis loop represents the energy consumption during a single cycle.

1.5.2. Losses through Néel and Brown relaxations

The relaxation losses can be induced through some relaxation processes which occur during the magnetization processes. In a magnetic ferrofluid, the magnetization reversal usually occurs through Brown or Néel relaxation processes. The

Néel relaxation concerns the rotation of the magnetic moment inside the particle and appears when the heat energy exceeds the energy barrier [11]. If the particle moves freely inside a liquid medium with viscosity η, a second relaxation mechanism appears due to the re-orientation of the entire particle. The mechanism concerns the Brown process [12].

Chapter II
Methods for the investigation of structural, magnetic and thermal properties of the magnetic powders with spinel structure

2.1. X-rays diffraction (XRD)

The X-rays diffraction is the mostly used technique to determine the crystallite dimensions, the spaces between the crystallographic planes, the directions of the diffraction planes, the presence of residual phases and the values of the lattice spacing of the crystalline materials.

2.2. Transmission electron microscopy

The operation of the transmission electron microscope is based on the effect of structural characteristics of the studied material. This produces images by focusing a high energy electron beam through a thin layered sample. The sample preparation for TEM analysis is an important stage and it usually demands its deposition on fine metal meshes or on a carbon support grid.

2.3. Energy Dispersive X-ray Spectroscopy (EDX)

The Energy Dispersive X-ray Spectroscopy (EDX) is an analytical technique used for elemental analysis and determination of the chemical composition of magnetic nanoparticles. From the EDX data one can estimate the ratio of the concentrations of the chemical elements from the sample [2]. A spectrometer attached to the transmission electron microscope forms the so-called analytic TEM microscope. The portable EDX systems were built using X-rays tubes or radioactive sources.

2.4. Dynamic light scattering (DLS)

Zetasizer is a device that performs measurements of microscopic particle size using the dynamic light scattering (DLS).

The dynamic light scattering, also known as Photon Correlation Spectroscopy (PCS), measures the scattering spectrum produced when light passes through a sample. This method is based on the calculus of the diffusion caused by the Brownian motion described by the Stokes- Einstein equation [13, 14].

2.5. Zeta potential

The values of the zeta potential show the stability of a colloidal system. A positive or negative value of 30 mV can be considered as an arbitrary value which indicates the colloid stability. In the case of a small particle, a zeta potential value that exceeds 30 mV (positive or negative) indicates the solution stability and the tendency of nanoparticles to remain dispersed. When smaller values of the zeta potential are recorded, the attraction exceeds the rejection and the phenomenon of particles agglomeration appears [15].

2.6. Fourier Transform Infrared Spectroscopy

The Fourier Transform Infrared Spectroscopy (FTIR) can be used for the investigation of the gaseous, liquid and solid materials at high or low temperatures. This technique is based on the interaction between the electromagnetic radiations and the sample and it reveals the nature of the vibration of chemical bonds between the atoms and molecules which compose the material. The FTIR spectra contain information concerning the presence of some functional groups/types of bonds in the molecules of the studied sample [16].

2.7. Vibration Magnetometry. Vibrating Sample Magnetometer (VSM)

The Vibrating Sample Magnetometer (VSM) was proposed by Simon Foner [17] in 1956. This efficient method for measurement and characterization of the magnetic material properties is based on the law of electromagnetic induction. Hysteresis loops of samples under various shapes in different configurations can be obtained [18].

2.8. Calorimetric method for the determination of specific absorption rate of colloidal suspensions

In order to measure the specific absorption rate of the studied colloidal suspensions (ferrofluids), a calorimetric technique for power absorption measurement was used [19]. By performing measurements of ferrofluid heating/cooling, one can obtain the values of sample temperatures (T) as function of time (t). For a better precision of the experimental data, the ferrofluid temperature measurements during heating and cooling is performed by means of a optical fiber thermometer with GaAs sensor.

All these methods of characterizations contributed to the determination of morphological, structural and magnetic properties and the determination of the specific absorption rate of $Mn_xFe_{1-x}Fe_2O_4$ and $Co_xFe_{1-x}Fe_2O_4$ nanoparticles studied in this work.

Chapter III

Contributions to the study of $Mn_xFe_{1-x}Fe_2O_4$ and $Co_xFe_{1-x}Fe_2O_4$ nanoparticles in aqueous solution

3.1. Contributions to the study of $Mn_xFe_{1-x}Fe_2O_4$ nanoparticles in aqueous solution

3.1.1. Production of $Mn_xFe_{1-x}Fe_2O_4$ nanoparticles in aqueous solution through co-precipitation method

In order to obtain colloidal suspensions of $Mn_xFe_{1-x}Fe_2O_4$ nanoparticles, with x varying from 0 to 1, a simple and convenient method was used, namely the co-precipitation method [20-23].

The poly-condensation of the (Fe^{3+}, Fe^{2+} and Mn^{2+}) cations from an aqueous solution in alkaline medium can be described by the relation [19]:

$$(1-x)Fe^{2+} + xMn^{2+} + 2Fe^{3+} + 8OH^{=} \rightarrow (1-x)Fe^{2+}(OH)_2 \cdot xMn(OH)_2 \cdot 2Fe(OH)_3 \downarrow \quad (3.1)$$

The conversion of the solid solution of the metallic hydroxides in manganese ferrite is accomplished through heating:

$$(1-x)Fe^{2+}(OH)_2 + xMn(OH)_2 + 2Fe(OH)_3 \rightarrow Mn_xFe_{(1-x)}Fe_2O_4 \cdot nH_2O + (4-n)H_2O \quad (3.2)$$

The general reaction of iron oxide nanoparticle formation can be described by the reaction:

$$(1-x)Fe^{2+} + xMn^{2+} + 2Fe^{3+} + 8OH^{-} \rightarrow Mn_xFe_{(1-x)}Fe_2O_4 \cdot nH_2O + (4-n)H_2O \quad (3.3)$$

where x is the molar percentage.

3.1.2. Study of structural properties of manganese ferrite nanoparticles

3.1.2.1. Results of the X-rays diffraction analysis of the $Mn_xFe_{1-x}Fe_2O_4$ nanoparticles

The X-rays diffraction analyses were carried out by means of the PANalytical, X'PertPro diffractometer (from the Laboratory of the Physical Chemistry Department of the Saarland University, Germany) with the CuK_α radiation (λ= 1.54059 Å, I= 40 mA, U= 45 kV) at room temperature, with a step of 0.02^o and 1 sec time for each step. From powders diffractograms (Figure 3.1) [24] one can notice the formation of a face centered cubic (FCC) structure of the $Mn_xFe_{1-x}Fe_2O_4$ ferrite for all the six values of x: 0, 0.2, 0.4, 0.6, 0.8 and 1 respectively.

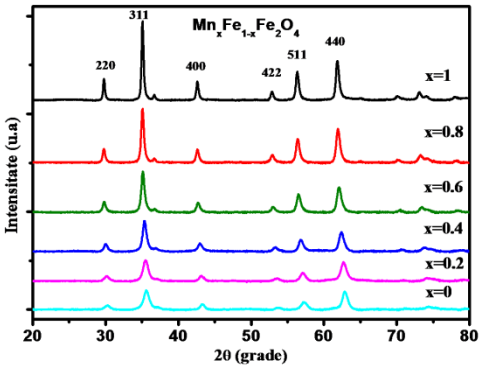

Figure 3.1. Diffractograms of the $Mn_xFe_{1-x}Fe_2O_4$ powders [24].

By using the peaks half-width and the Scherrer equation [25], the average value of the crystallite size was determined (Table 3.3). It was noticed that the crystallite dimension increased with increasing level of iron substitution by manganese. This increase from 9 to 16 nm was due to the size of ionic radius, the Fe^{3+} ionic radius (0.63Å) [26] being smaller than the radius of Mn^{2+} ion (0.81 Å)[27].

3.1.2.2. *Results of the TEM microscopy and EDX analysis of the elemental composition of $Mn_xFe_{1-x}Fe_2O_4$ nanoparticles*

The images from the transmission electron microscopy (Figure 3.4), taken over by the Jeo Jem 2010 device from the Laboratory of the Physical Chemistry Department of the Saarland University, Germany offered the possibility to determine nanoparticles shape, dimension and agglomeration degree. From the TEM images, one can notice the groups of faceted nanoparticles of various shapes (polyhedral or almost spherical). The average size of the $Mn_xFe_{1-x}Fe_2O_4$ nanoparticles was determined by using the Image J Software and measuring the dimensions of at least 50 particles. The obtained values are in nanometer range, between 10.5 and 21.2 nm.

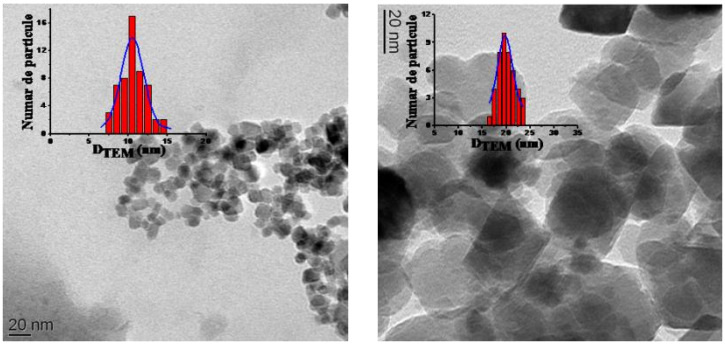

(a) (f)

Figure 3.4. TEM images for nanoparticles of: a) Fe_3O_4 and f) $MnFe_2O_4$ [24].

By comparing these results with XRD results, one can draw the conclusion that the nanoparticles are of the dimension of a single magnetic domain. One can notice that the particle dimension increases with the increase of the level of Fe substitution by Mn.

By means of the energy dispersive X-rays spectrophotometer (EDX) one could determine the elemental composition of the magnetic nanoparticles. The EDX analysis confirms the presence of the chemical metallic elements Fe and Mn.

3.1.2.3. *Results of the DLS analysis of $Mn_xFe_{1-x}Fe_2O_4$ nanoparticles*

In order to determine the hydrodynamic diameter (D_{hydro}) and particle distribution according to their size, a Zetasizer Nano ZS device from Malvern Instruments was used, based on the process of dynamic light scattering. In order to record the values of the dynamic diameter and the distribution of magnetic nanoparticles, the particle suspension was measured five times at room temperature and the average value was taken into account. The obtained values ranged between 75nm and 110 nm. According to Kin researches [28], the high values of the hydrodynamic diameter can be explained through the nanoparticles tendency to agglomerate into the aqueous suspension.

3.1.2.4. *Results of the vibration spectral analysis of $Mn_xFe_{1-x}Fe_2O_4$ nanoparticles*

The FTIR analysis was used in nanoparticles case to identify the vibrations corresponding to metal- oxygen bond from the crystallographic positions corresponding to the structure of spinel, tetrahedral and octahedral type respectively, taking into account that each cation has its own coordination mode.

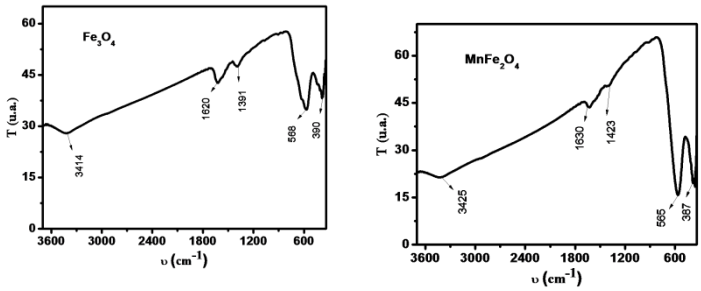

(a) (f)

Figura 3.7. FTIR spectra for nanoparticles of: a) Fe_3O_4 and f) $MnFe_2O_4$.

Two vibration peaks characteristic to carboxyl group, -COO-, which belong to the sodium citrate were detected between 1620- 1630 cm^{-1} and 1391- 1423 cm^{-1}. The strong absorption maxima noticed within the interval 564- 569 cm^{-1} are assigned to intrinsic stretching vibrations of the bonds between the metal ions

and oxygen ions from the tetrahedral positions, while the weak absorption maxima correspond to the stretching vibrations of the bonds between the metal ions and oxygen ions from the octahedral positions [29, 30]. Weak absorption peaks are noticed within the interval 383- 390 cm^{-1}. According to Waldron study [34], one can state that these two absorption peaks suggest the generation of the spinel structure of the manganese ferrite nanoparticles.

3.1.3. Magnetic properties of the $Mn_xFe_{1-x}Fe_2O_4$ ferrite

The measurements of the magnetic properties of the $Mn_xFe_{1-x}Fe_2O_4$ powders were performed at room temperature with vibrating sample magnetometer Lake Shore Model 7300. The hysteresis loops were recorded in a continuous magnetic field varied between -20 kOe and +20 kOe. From the magnetization curve, M vs. H, one can determine the superparamagnetic behavior of the entire series of $Mn_xFe_{1-x}Fe_2O_4$. This can be explained by the small particle size, a result confirmed by the TEM analysis.

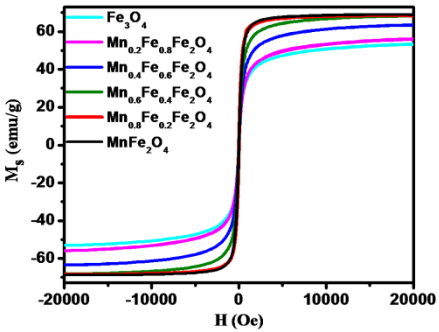

Figure 3.8. Magnetization curves at room temperatures for nanoparticles from $Mn_xFe_{1-x}Fe_2O_4$ series [24].

One can notice a monotonous increase of the saturation magnetization with x (level of iron substitution by manganese), but for x= 0.6, 0.8 and 1 the magnetization values are just about the same. This magnetization behavior cannot be explained only by the cations distribution, but also by the particle dimension and the so-called “spin canting” effect [27, 33]. The obtained values are smaller

than those characteristic to the bulk materials (110.6 emu/g) [34], due to the small particle dimensions and the synthesis method.

3.2. Contributions to the study of $Co_xFe_{1-x}Fe_2O_4$ nanoparticles in aqueous solution

3.2.1. Production of $Co_xFe_{1-x}Fe_2O_{4p}$ particles in aqueous solution through co-precipitation method

The $Co_xFe_{1-x}Fe_2O_4$ nanoparticles, with x varying from 0.1 to 1, were prepared through co-precipitation method, the same synthesis method as in the case of manganese nanoparticles.

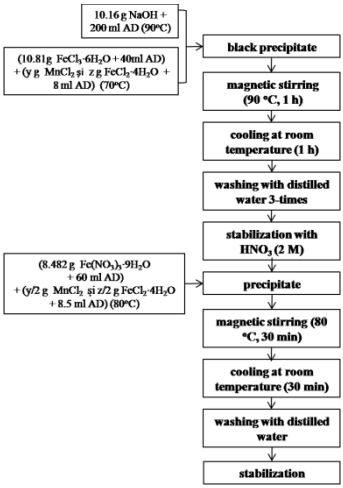

Figure 3.11. Schematic diagram of $Co_xFe_{1-x}Fe_2O_4$ nanoparticles synthesis method

3.2.2. Study of the structural properties of the nanoparticles of cobalt ferrite

3.2.2.1. Results of X-rays diffraction analysis of the $Co_xFe_{1-x}Fe_2O_4$ nanoparticles

These diffractograms confirmed the formation of a face centered cubic (FCC) structure characteristic to the $Co_xFe_{1-x}Fe_2O_4$ ferrite, for all the six values of x: 0, 0.2, 0.4, 0.6, 0.8, 1. The dimensions of the crystallites of nanoparticles from the cobalt ferrite

series were determined by using the *Origin* software and a Lorentz deconvolution of the diffraction data.

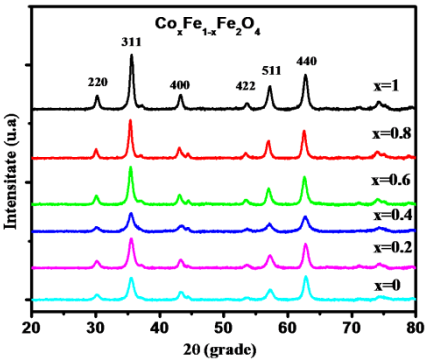

Figure 3.12. Diffractograms of the $Co_xFe_{1-x}Fe_2O_4$ powders [37].

The experimental data proved that the crystallite dimensions increase with increasing level of iron substitution by cobalt, except for the sample with x= 0.4, for which crystallite size remains the same as for magnetite. This noticed increase of the crystallites size from 9.1 to 15.5 nm can be explained by the substitution of Fe^{2+} ion, with a smaller atomic ray (0.61Å) by the Co^{2+} ions, with a little bigger radius (0.62Å) [28, 37].

3.2.2.2. Results of TEM microscopy and EDX analysis of the elemental composition of $Co_xFe_{1-x}Fe_2O_4$ nanoparticles

As in the case of manganese nanoparticles, the transmission electron microscopy images (JEOl JEM 2010) gave the possibility to determine the nanoparticles shape, dimension and agglomeration degree.

The average dimensions of the $Co_xFe_{1-x}Fe_2O_4$ nanoparticles were determined by using the ImageJ software, measuring the dimension of at least 100 particles. The obtained values are within the nanometer range, between 8.6 and 15.7 nm (Table 3.11). These values are comparable with the average dimensions of the crystallites, which suggest that the nanoparticles are magnetic single domains.

Table 3.11. Particle size and hydrodynamic dimension of $Co_xFe_{1-x}Fe_2O_4$ nanoparticles [37].

	D_{TEM} (nm)	D_{hidro} (nm)
Fe_3O_4	10.7 ± 0.1	61 ± 2
$Co_{0.2}Fe_{0.8}Fe_2O_4$	10.8 ± 0.1	57 ± 2
$Co_{0.4}Fe_{0.6}Fe_2O_4$	9.6 ± 0.1	51 ± 2
$Co_{0.6}Fe_{0.4}Fe_2O_4$	13.7 ± 0.2	55 ± 2
$Co_{0.8}Fe_{0.2}Fe_2O_4$	14.6 ± 0.2	63 ± 2
$CoFe_2O_4$	15.7 ± 0.2	75 ± 2

3.2.2.3. Results of the DLS analysis of $Co_xFe_{1-x}Fe_2O_4$ nanoparticles [37]

In order to determine the hydrodynamic diameter (D_{hydro}) of the cobalt particles we have used the same device (Zetasizer Nano ZS from Malvern Instruments) and the same experimental conditions as in the case of manganese nanoparticles. The obtained results indicated hydrodynamic diameters ranging between 51 and 57 nm (Table 3.11). As in the case of $Mn_xFe_{1-x}Fe_2O_4$ ferrite, one can notice high values of the hydrodynamic diameter, which can be the result of nanoparticles agglomeration in aqueous suspensions.

3.2.2.4. Results of the vibration spectral analysis of $Co_xFe_{1-x}Fe_2O_4$ nanoparticles

The FTIR spectrum was recorded in this case too by means of the Jasco Plus 660 instrument, an infrared spectrophotometer. The magnetic nanoparticles were dispersed in KBr.

The weak intensity absorption bands noticed within the interval 383- 390 cm^{-1} are associated with the stretching vibrations of the bonds between the metal and oxygen ions from octahedral positions [31, 32]. The strong absorption bands noticed within the interval 564- 569 cm^{-1} are assigned to the stretching vibrations of the bonds between the metal and oxygen ions from tetrahedral positions. It follows that the absorption maxima produced around 390 and 570 cm^{-1} confirm the formation of spinel-type structure of the cobalt ferrite nanoparticles, according to Waldron study [33].

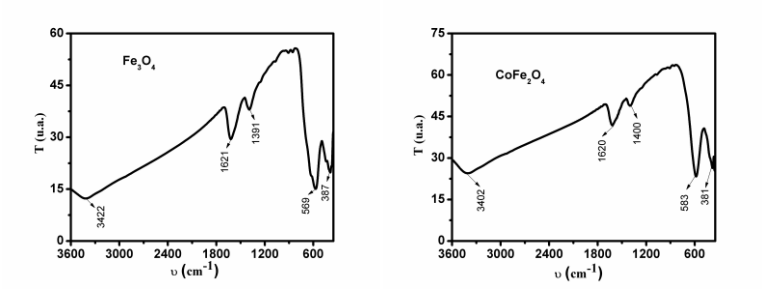

Figure 3.18. FTIR spectrum of nanoparticles of (a) Fe_3O_4 and (f) $CoFe_2O_4$.

3.2.3. Magnetic properties of the $Co_xFe_{1-x}Fe_2O_4$ ferrite

The hysteresis loops of the $Co_xFe_{1-x}Fe_2O_4$ nanoparticles powders are presented in Figure 3.19. From the magnetization curves M vs. H, one can notice that the transition from the superparamagnetic behavior to ferromagnetic behavior occurs with the increase of the cobalt content in the $Co_xFe_{1-x}Fe_2O_4$ ferrite.

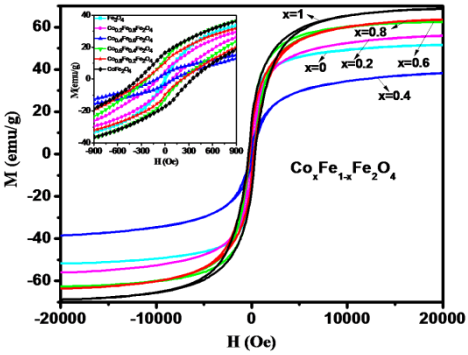

Figure 3.19. The magnetization curves of the $Co_xFe_{1-x}Fe_2O_4$ series at room temperature [34].

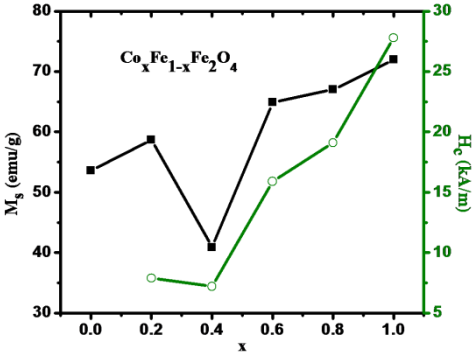

Figure 3.20. Saturation magnetization (M_s) and coercive force (H_c) vs. cobalt content (x) for the $Co_xFe_{1-x}Fe_2O_4$ series.

The values of the saturation magnetization (M_s) of the $Co_xFe_{1-x}Fe_2O_4$ powders were estimated through the representation and interpolation of the magnetization as function of the reciprocal of the magnetic field (1/H). The values of the coercive force (H_c) and the saturation magnetization were graphically represented in terms of the cobalt content in Figure 3.20. One can notice the increase of the saturation magnetization and coercive force with the increase of the level of iron substitution by cobalt, but for x= 0.4 these show a decrease. The $Co_xFe_{1-x}Fe_2O_4$ nanoparticles these decrease due to the smaller crystallite and particle dimensions.

Conclusions

- We obtained through co-precipitation aqueous ferrofluids with the chemical formula $Mn_xFe_{1-x}Fe_2O_4$ and $Co_xFe_{1-x}Fe_2O_4$ with x= 0, 0.2, 0.4, 0.6, 0.8, and 1.
- The XRD diffractograms confirmed the spinel structure of all the nanoparticles from the both series.
- The TEM images confirmed the nanoparticles dimension of nanometer order, while the crystallite dimension computed through XRD suggested that most of the nanoparticles are single magnetic domains
- The superparamagnetic behavior was deduced from the magnetization curves of the $Mn_xFe_{1-x}Fe_2O_4$ series,

explained through the small dimension of crystallite and particles respectively. The hysteresis loops measured for $Co_xFe_{1-x}Fe_2O_4$ indicated the passage from the superparamagnetic behavior to the ferrimagnetic behavior when increasing the level of iron substitution by cobalt.

CHAPTER IV
Contributions to the study of specific absorption rate of $Mn_xFe_{1-x}Fe_2O_4$, $Co_xFe_{1-x}Fe_2O_4$ and $Co_xFe_{1-x}Fe_2O_4$ nanoparticles dispersed in aqueous solution

4.1. Determination of the specific absorption rate of $Mn_xFe_{1-x}Fe_2O_4$ based ferrofluids

In order to accomplish the correspondence between the properties of the nanoparticles with the formula $Mn_xFe_{1-x}Fe_2O_4$ and the specific absorption rate of ferrofluids produced with them, we resorted to the determination of SAR using a calorimetric method described in Chapter II, Section 2.8. Through this method we performed measurements to determine the temperature variation in time.

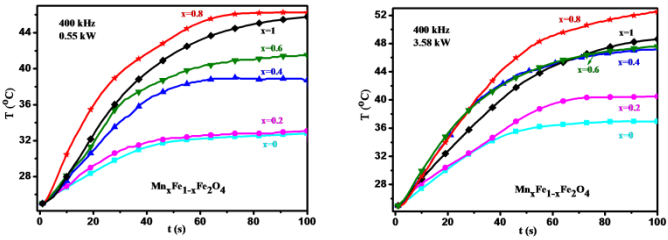

(a) (f)

Figure 4.3. Temperature variation in time for the $Mn_xFe_{1-x}Fe_2O_4$ series at powers of (a) 0.55 kW and (f) 3.58 kW at the frequency of 400 kHz.

One can notice that the maximum temperature reached by the ferrofluid depends on the chosen frequency, being much higher in the case of the frequency of 1950 kHz. This is mainly due to the magnetic relaxation mechanisms that occur. In the case of nanoparticles dispersion in water based fluids, the Néel relaxation prevails. This shows that the time interval when the temperature increase to the maximum value is different at the two frequencies.

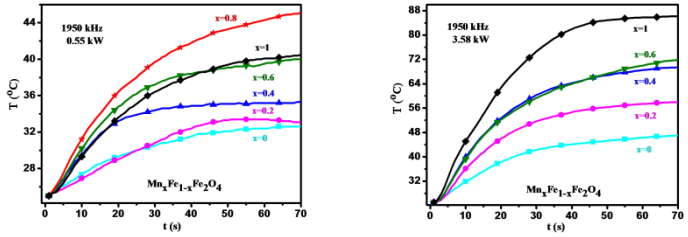

(a) (f)

Figure 4.4. Temperature variation in time for the $Mn_xFe_{1-x}Fe_2O_4$ series at powers of (a) 0.55 kW and (f) 3.58 kW at the frequency of 1950 kHz [24]

Making use of the relation 4.3 [36] and the slope of the temperature curve (Figures 4.3 and 4.4), one can obtain the values of the specific absorption rate :

$$SAR = C\frac{1}{m_{NP}}\frac{dT}{dt} \qquad (4.3)$$

where:

- C is the specific heat of the entire sample
- m_{NP} is the content of nanoparticles from the ferrofluid
- dT/dt is the temperature variation rate.

The ferrofluid specific heat was calculated with the formula:

$$C = \frac{m_{Mn_xFe_{1-x}Fe_2O_4} C_{Mn_xFe_{1-x}Fe_2O_4} + m_{water} C_{water}}{m_{Mn_xFe_{1-x}Fe_2O_4} + m_{water}} \qquad (4.4)$$

where:

- $m_{Mn_xFe_{1-x}Fe_2O_4}$ and m_{water} represent the mass of $Mn_xFe_{1-x}Fe_2O_4$ nanoparticles from the ferrofluid and the quantity of the utilized water respectively;
- $C_{Mn_xFe_{1-x}Fe_2O_4}$ and C_{water} represent the specific heats of the $Mn_xFe_{1-x}Fe_2O_4$ nanoparticles and water respectively .

According to the results reported by other researchers [36], the graphic presents a linear variation of SAR with the magnetic field power. This dependence is justified by the mechanism of Néel relaxation losses and can also be associated with the composition of the nanoparticles content from the ferrofluid. One can notice that the values of the specific absorption rate reached by the ferrofluid depend on the selected frequency, being much higher in the case of the frequency of 1950 kHz. An atypical behavior is remarked for the

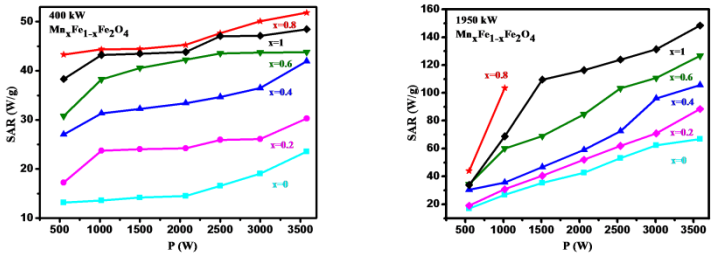

(a) (b)

Figure 4.6. Variation of the specific absorption rate (SAR) with the power (P) at the frequency of (a) 400 kHz, and (b) 1950 kHz for the $Mn_xFe_{1-x}Fe_2O_4$ series [24].

case x= 0.8 in the case of the frequency of 1950 kHz, which led to SAR determination only for two values of the power (0.55 and 1.02 kW). The values of the specific absorption rate obtained for $Mn_{0.8}Fe_{0.2}Fe_2O_4$ are much bigger than for Mn Fe_2O_4, even if the values of the magnetic moments and the average particles sizes are comparable. Since the prevailing relaxation mechanisms are the Néel losses, one can conclude, as in other studies [36, 37], that the anisotropy constant plays the determinant role.

4.2. Determination of the specific absorption rate for $Co_xFe_{1-x}Fe_2O_4$ ferrite-based ferrofluids

As in the case of $Mn_xFe_{1-x}Fe_2O_4$ nanoparticles, the temperature variation in time was determined, carrying out measurements by means of the same calorimetric method. The temperature variation in time for different powers of the applied magnetic field at the frequencies of 400 kHz and 1950 kHz for $Co_xFe_{1-x}Fe_2O_4$ nanoparticles, with x= 0÷1 are presented in Figures 4.10 and 4.11. From these curves one can notice a direct proportionality between the magnetic field power and the temperature of each ferrofluid.

As in the case of $Mn_xFe_{1-x}Fe_2O_4$ nanoparticles, the maximum temperature reached by the ferrofluid depends on the generator frequency. The obtained results show that at 400 kHz the recorded temperatures were much higher. The heating in the case of these Cobalt nanoparticles is also due to the hysteresis losses. The analysis of these curves also shows that the time while the

temperature increases to its maximum values varies with frequency, smaller time intervals being necessary at the frequency of 400 kHz [24, 37].

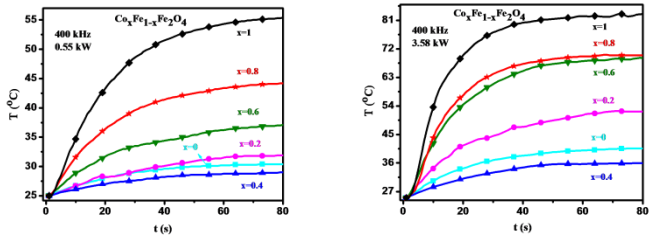

(a) (e)

Figure 4.10. Temperature variation in time for the $Co_xFe_{1-x}Fe_2O_4$ series at powers of (a) 0.55 kW and (e) 3.58 kW at the frequency of 400 kHz [34].

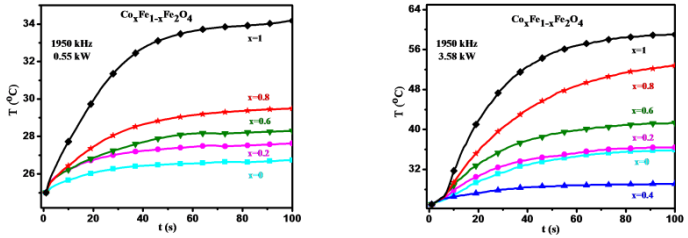

(a) (e)

Figure 4.11. Temperature variation in time for the $Co_xFe_{1-x}Fe_2O_4$ series at powers of (a) 0.55 kW and (e) 3.58 kW at the frequency of 1950 kHz [34]

One can notice that the obtained values are much higher values at low frequencies (400 kHz) than in the case of 1950 kHz. In the case of $Co_{0.4}Fe_{0.6}Fe_2O_4$ nanoparticles, a decrease of the specific absorption rate was found at both frequencies. The resulted SAR values ranged between 12 and 29.3 W/g for the frequency of 400 kHz. What concerns the SAR determination at the frequency of 1950 kHz, this was only carried out for powers exceeding 2050 W. These smaller SAR values correspond to the small values of crystallite and particle dimensions, as well as of the saturation magnetization.

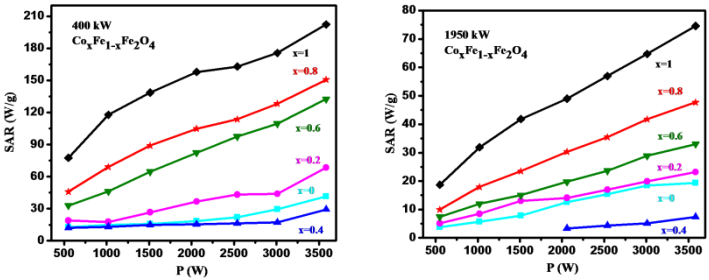

(a) (b)

Figure 4.13. Variation of the specific absorption rate (SAR) with the power (P) for different powers at frequencies of (a) 400 kHz and (b) 1950 kHz for $Co_xFe_{1-x}Fe_2O_4$ series

4.3. Determination of the specific absorption rate of ferrofluids based on $Zn_xCo_{1-x}Fe_2O_4$ ferrite

The magnetic $Zn_xCo_{1-x}Fe_2O_4$ nanoparticles represented the objective of the investigations concerning the specific absorption rate, but not the structural and magnetic properties. The temperature vs. time curves were recorded for the frequencies of 400 kHz and 1950 kHz using the same calorimetric method and the same experimental conditions as those used in the case of manganese and cobalt.

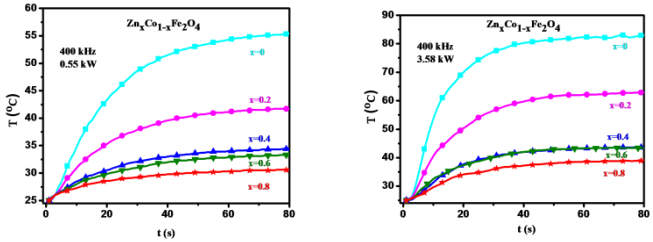

(a) (e)

Figure 4.18. Temperature variation with time for the $Zn_xCo_{1-x}Fe_2O_4$ series at power values of (a) 0.55 kW and (e) 3.58 kW at the frequency of 400 kHz [38].

From the analysis of these curves one can notice a straightforward proportionality between the magnetic field power and the temperature of each ferrofluid.

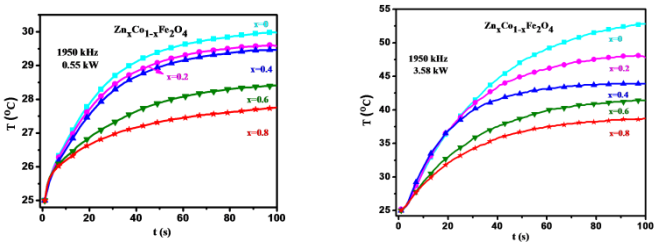

(a) (e)

Figure 4.19. Temperature variation with time for the $Zn_xCo_{1-x}Fe_2O_4$ series at power values of (a) 0.55 kW and (e) 3.58 kW at the frequency of 1950 kHz [38].

As in the case of $Mn_xFe_{1-x}Fe_2O_4$ and $Co_xFe_{1-x}Fe_2O_4$ nanoparticles, the maximum temperature that the ferrofluid can reach depends on the generator frequency. The obtained results show that at the frequency of 400 kHz the recorded temperatures were much higher. The analysis of these curves also shows that another important factor in reaching the maximum temperature is the Zn quantity introduced in the lattice [38]. The higher the Zn quantity introduced in the lattice, the lower the temperature values.

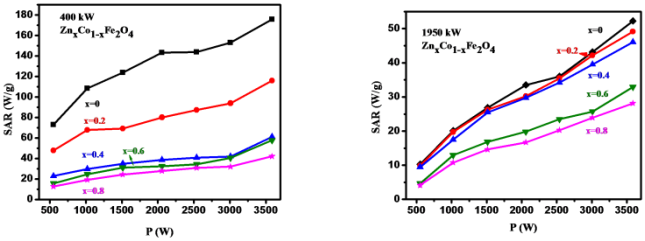

(a) (b)

Figure 4.20. Variation of the specific absorption rate (SAR) with the power (P) for different powers at the frequency of (a) 400 kHz and (b) 1950 kHz for the $Zn_xCo_{1-x}Fe_2O_4$ series [38].

One can notice that the maximum values of the specific absorption rate are obtained at low frequency (400 kHz), as in the case of the magnetic $Co_xFe_{1-x}Fe_2O_4$ nanoparticles. A decrease of the specific absorption rate was noticed in the case of both frequencies in the case of Zn substitution in the lattice. The small values of SAR correspond to the small values of crystallite and particle dimensions, as well as of the saturation magnetization and coercive force [38].

4.4. Comparative study of $Mn_xFe_{1-x}Fe_2O_4$ and $Co_xFe_{1-x}Fe_2O_4$ nanoparticles used in hyperthermia

In this sub-chapter we proposed to accomplish a comparative study of the $Mn_xFe_{1-x}Fe_2O_4$, $Co_xFe_{1-x}Fe_2O_4$ and $Co_xFe_{1-x}Fe_2O_4$ ferrites (x= 0÷1) with possible applications in magnetic hyperthermia. The nanoparticle systems were synthesized using the same synthesis method, i.e. co-precipitation method, while maintaining the same synthesis parameters.

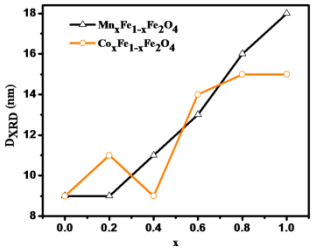

Figura 4.22 Variation of crystallite dimension in terms of the manganese and cobalt quantities from the $Mn_xFe_{1-x}Fe_2O_4$ and $Co_xFe_{1-x}Fe_2O_4$ series respectively

The XRD diffractograms revealed the formation of spinel structure for all the series members, which confirms the introduction of manganese and cobalt respectively into the crystalline lattice. Figure 4.22 presents the variation of the crystallite dimension as function of manganese and cobalt quantities in the case of $Mn_xFe_{1-x}Fe_2O_4$ and $Co_xFe_{1-x}Fe_2O_4$ particles respectively. The experimental data proved that the values of crystallite dimension are comparable, ranging between 8.9 ÷18.2 nm and 9.1÷ 15.7 nm respectively.

Table 4.5. Saturation magnetization (M_s) and coercive field (H_c) of $Mn_xFe_{1-x}Fe_2O_4$ and $Co_xFe_{1-x}Fe_2O_4$ nanoparticles [24, 34]

x	$Mn_xFe_{1-x}Fe_2O_4$	$Co_xFe_{1-x}Fe_2O_4$	
	M_s (emu/g)	Ms (emu/g)	H_C (Oe)
0	53.4	51.6	0.07
0.2	56.3	55.8	99.27
0.4	63.3	38.2	90.47
0.6	68.2	62.4	199.80
0.8	68.7	63.5	240.01
1	68.8	68.6	349.34

The saturation magnetization and coercive force of each series member were determined from the magnetic measurements of the manganese and cobalt powders. The values of saturation magnetization and coercive force for each sample are given in Table 4.5. One can notice an increase of magnetization with the increasing amount of manganese and cobalt introduced in the lattice. The highest value of the saturation magnetization was registered for x= 1 in the case of both series. The results obtained for the saturation magnetization of the $Mn_xFe_{1-x}Fe_2O_4$ and $Co_xFe_{1-x}Fe_2O_4$ nanoparticles are comparable. The lowest value of M_s for x= 0.4 can be accounted for by the diminution of the crystallite and particle dimensions.

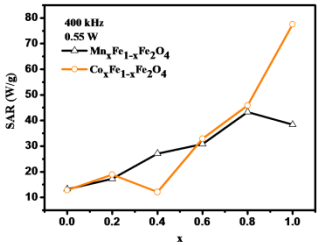

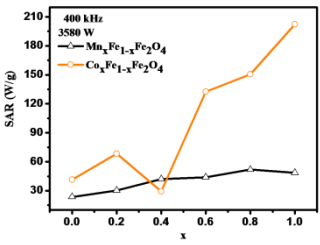

(a) (e)

Figure 4.24. Variation of the specific absorption rate (SAR) as function of manganese and cobalt content (x) from the $Mn_xFe_{1-x}Fe_2O_4$ and $Co_xFe_{1-x}Fe_2O_4$ series respectively at the frequencies of 400 kHz at magnetic field powers of (a) 0.55 kW and (e) 3.58 kW.

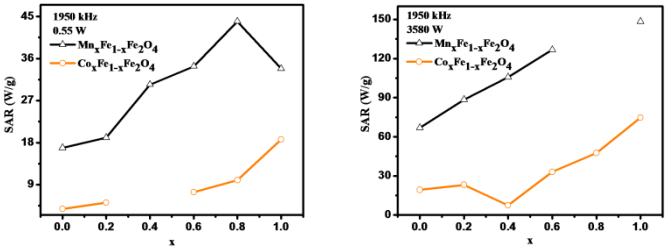

(a) (e)

Figure 4.25. Variation of the specific absorption rate (SAR) as function of manganese and cobalt content (x) from the $Mn_xFe_{1-x}Fe_2O_4$ and $Co_xFe_{1-x}Fe_2O_4$ series respectively at the frequencies of 1950 kHz at magnetic field powers of (a) 0.55 kW and (e) 3.58 kW.

The variation of the specific absorption rate (SAR) as function of manganese and cobalt content (x) from the $Mn_xFe_{1-x}Fe_2O_4$ and $Co_xFe_{1-x}Fe_2O_4$ series respectively at the frequencies of 400 kHz and 1950 kHz and at different powers of the applied magnetic field are presented in Figures 4.24 and 4.25 respectively. The two nanoparticles series present increases of the specific absorption rate with the increase of the applied magnetic field. One can notice that the results obtained for the cobalt ferrite are higher than those for the manganese ferrite at the frequency of 400 kHz and lower at the frequency of 1950 kHz.

From the above presentation, one can remark that the values of the specific absorption rate depend on the particles structural and magnetic properties, as well as on the applied magnetic field frequency and intensity.

Conclusions

- An increase of SAR with the increase of the level of manganese and cobalt substitution was noticed.

- At the frequency of 400 kHz for the manganese series the obtained values were much lower than at high frequency, the maximum values being determined for $Mn_{0.8}Fe_{0.2}Fe_2O_4$.
- The specific absorption rate determined for $Co_xFe_{1-x}Fe_2O_4$ series had its maximum value at the frequency of 400 kHz, this varying when the magnetic field power changes. The highest SAR value (202.2 W/g) was registered for $CoFe_2O_4$ at a field power of 3.58 kW at the frequency of 400 kHz.
- The experimental data revealed a straightforward proportionality between the values of specific absorption rate and the crystallite dimension, the average particle dimension and the saturation magnetization.

GENERAL CONCLUSIONS

The experimental results presented and detailed in this dissertation bring their contributions to the study of magnetic nanoparticles of manganese and cobalt ferrites, obtained through the method of chemical precipitation. We investigated the influence of iron substitution with manganese and cobalt on the structural, morphological and magnetic properties of the magnetic manganese and cobalt nanoparticles. Still another important point was represented by the determination of the specific absorption rate (SAR) by means of the calorimetric method and the influence of structural and magnetic properties on its values.

With these objectives in view, magnetic nanoparticles of $Mn_xFe_{1-x}Fe_2O_4$ and $Co_xFe_{1-x}Fe_2O_4$ were obtained for various values of x using the method of chemical co-precipitation. The X-rays diffractograms demonstrated the formation of spinel structure, and the obtained calculated crystalline dimension was in the nanometer range. The crystalline dimension increased with the increase of the level of iron substitution by manganese and cobalt respectively, maximum values being obtained for x= 1. From the TEM images of the powders of manganese ferrite series we could notice groups of nanoparticles of various shapes (polyhedral or almost spherical). In the case of cobalt nanoparticles, the obtained shape was cubical.

From the analysis of the FTIR spectra of the magnetic ferrofluid samples one could notice the existence of peaks corresponding to the spinel structure, the presence of water traces

from the sample, and the formation of ions specific to the molecules of stabilizer at the particle surface.

Due to the small dimensions of crystallites and particles, the ferrite nanoparticles from the $Mn_xFe_{1-x}Fe_2O_4$ series have a superparamagnetic behavior. The highest value of the saturation magnetization was obtained in the case of $MnFe_2O_4$, while the smallest was obtained for magnetite (Fe_3O_4). From the analysis of the hysteresis loop of the $Co_xFe_{1-x}Fe_2O_4$ ferrites, one could notice the consolidation of the ferrimagnetic behavior with the increase of cobalt quantity introduced into the lattice. The sample saturation magnetization and coercive force increase with increasing level of iron substitution by cobalt. The maximum values were obtained for the highest cobalt amount (x=1).

We determined the temperature variation with time for manganese and cobalt ferrites using a calorimetric method. In this study the specific absorption rates of the manganese particles determined at high frequency (1950 kHz) are reported for the first time. What concerns the $Co_xFe_{1-x}Fe_2O_4$ ferrite, this is the first time that the specific absorption rates have been determined at the frequencies of 400 and 1950 kHz. The study highlights the importance of different factors, such as the chemical composition, the cation distribution, the average crystallite and particle dimensions, as well as the intensity and frequency of the applied magnetic field on the SAR values. The experimental data confirmed that the manganese ferrite presented the maximum SAR values at the frequency of 1950 kHz, while for the cobalt ferrite the maximum values were obtained at 400 kHz.

Literature

[1] A.H. Lu, E.L. Salabas, F. Schüth, *Magnetic nanoparticles: synthesis, protection, functionalization and application*, Angew. Chem. Int. Ed. 46 (2007) 1222-1244.

[2] M. Faraji, Y. Yamini, M. Rezaee, *Magnetic nanoparticles: synthesis, stabilization, functionalization, characterization and applications*, J. Iran. Chem. Soc. 1 (2010) 1-37.

[3] A. Chichel, J. Skowronek, M. Kubaszewska, M. Kanikowski, *Hyperthermia – description of a method and a review of clinical applications, Rep. Pract. Oncol. Radiother*. 12 (2007) 267-275.

[4] V.N. Nikiforov, *Magnetic induction hyperthemia*, Russian Physics Journal 50 (2007) 913-924.

[5] S.P. Gubin, Yu.A. Koksharov, G.B. Khomutov, G.Yu Yurkov, *Magnetic nanoparticles: preparation, structure and properties*, Russian Chemical Review 74 (6) (2005) 489 – 520.
[6] V. Mohite, *Self controlled magnetic hyperthermia*, Electronic These, Treatises and Dissertations, Department of mechanical engineering (2004).
[7] C.C. Berry, A.S.G. Curtis, *Funtionalisation of magnetic nanoparticles for applications in biomedicine*, J. Phys. D: Appl. Phys. 36 (2003) R198-R206.
[8] Q.A. Pankhurst, J. Connolly, S.K. Jones, J. Dobson, *Applications of magnetic nanoparticles in biomedicine*, J. Phys. D: Appl.Phys. 36 (2003) R167-R181.
[9] P. Pradhan, J. Giri, G. Samanta, H. D. Sarma, K. P. Mishra, J. Bellare, R. Banerjee, D. Bahadur, *Comparative evaluation of heating ability and biocompatibility of different ferrite-based magnetic fluids for hyperthermia application*, J Biomed Mater Res Part B: Appl Biomater 81B (2007) 12-22.
[10] M. Ma, Y. Wu, J. Zhou, Y. Sun, Y. Zhang, N. Gu, *Size dependence of specific power absorption of Fe3O4 particles in AC magnetic field*, J. Mag. Mag. Mater. 268 (2004) 33-39.
[11] A.H. Habib, C.L. Ondeck, P.Chaudhary, M.R.Bockstaller, M.E. McHenry, *Evaluation pf iron-cobalt/ferrite core-shell nanoparticles for cancer thermotherapy*, J. Appl. Phys 103(2008) 07A307.
[12] G. Glock, R. Hergt, M. zeisberger, S. Dutz, S. Nagel, W. Weitschies, *The effect of field parameters, nanoparticle properties and immobilization on the specific heating power in magnetic particle hyperthermia*, J. Phys.: Condens. Matter 18 (2006) S2935–S2949.
[13] S. Odenbach, *Colloidal Magnetic Fluids: Basic, Development and Application of Ferrofluids*, Pringer, Berlin Heidelberg (2009).
[14] S. Behrens, H. Bönnemann, N. Matoussevitch, H. Modrow, V. Kempter, W. Riehemann, A. Wiedenmann, S. Odenbach, S. Will, D. Eberbeck, R. Hergt, R. Müller, K. Landfester, A. Schmidt, D. Schüler, R. Hempelmann, *Synthesis and characterization*, Lect. Notes Phys. 763 (2009) 1-82.
[15] Technical note: *Zeta potential. An introduction in 30 minutes.* Malvern Instruments Ltd.
[16] M.Aluas, S. Simon, *Metode experimentale avansate pentru studiul și analiza bio-nano-sistemelor*, Editura Casa Cărții de Știință Cluj-Napoca (2012).
[17] S. Foner, *Versatile and sensitive Vibrating-Sample Magnetometer*, The Review of Scientific Instruments 30 (7) (1959) 548-557.
[18] W. Burgei, M.J. Pechan, H. Jaeger, *A simple vibrating smaple magnetometr for use in a meterials physics course*, Am. J. Phys. 71 (8) (2003) 825-828.
[19] V. Nica, H.M. Sauer, J. Embs, R. Hempelmann, *Calorimetric method for determination of Curie temperatures of magnetic nanopartices in dispersion*, J. Phys.: Condens. Matter 20 (2008) 204115 1-5.
[20] R. Massart, *Preparation of aqueous magnetic liquids in alkaline and acidic media*, IEEE Trans. Magn. 17 (1981) 1247-1248.
[21] D. Zins, V. Cabuil, R. Massart, *New aqueous magnetic fluids*, J. Mo. Liq. 83 (1999) 217-232.
[22] X. Le Guével, E-M. Prinz, R. Müller, R. Hempelmann, M. Schneider, *Synthesis and characterization of superparamagnetic nanoparticles coated with fluorescent gold nanoclusters*, J. Nanopart. Res. 14 (2012) 727-737,

[23] A.M. Cojocariu, **A. Doaga**, W. Amin, P. Bender, R. Hempelmann, O.F. Caltun, *Synthesis and functionalization of magnetic nanoparticles with possible application in drug delivery systems*, Dig. J. Nanomater. Bios. 8 (2013) 519-527.
[24] **A. Doaga**, A.M. Cojocariu, W. Amin, F. Heib, P. Bender, R. Hempelmann, O.F. Caltun, *Synthesis and characterizations of manganese ferrites for hyperthermia applications*, trimis spre publicare la Mat. Chem. Phys.
[25] S.M. Attia, *Study of cation distribution of Mn-Zn Ferites*, Egypt. J. Solid 29 (2006) 329-340.
[26] R.D. Shannon, *Revised effective ionic radii and systematic studies of interatomic distances in halides and chalcogenides*, Acta Cryst. A32 (1976) 751-767.
[27] R.V. Upadhyay, K.J .Davies, S. Well, S.W. Charles, *Preparation and characterization of ultra-fine $MnFe_2O_4$ and $Mn_xFe_{1-x}Fe_2O_4$ spinel systems: I. particles*, J. Magn. Magn. Mater. 132 (1994) 249-257.
[28] D. H. Kim, D. E. Nikles, C. S. Brazel, *Synthesis and characterization of multifunctional chitosan $MnFe_2O_4$ nanoparticles for magnetic hyperthermia and drug delivery*, Material 3 (2010) 4051-4065.
[29] A.M. Cojocariu, M. Soroceanu, L. Hrib, V. Nica, O.F. Caltun, *Microstructure and magnetic properties of substituted (Cr, Mn) – cobalt ferrite nanoparticles*, Mat. Chem. Phys. 135 (2012) 728-732.
[30] S.A. Mazen, H.M. Zaki, S.F. mansour, *Infrared absorption and dielectric properties of Mg-Zn ferrite*, *International journal of pure and applied physics* 3 (2007) 40-48.
[31] R.D. Waldron, *Infrared spectra of ferrites*, Physical review 99 (1955) 1727-1735.
[32] K.S. Lohar, S.M. Patange, S.E. Shirsath, V.S. Surywanshi, S.S. gaikwad, S.S. Jadhav, N. Kulkarni, *Structural refinement by rietveld method and magnetic study of nano-crystalline Cu-Zn*, International Journal of Advances in Engineering&Technology 3 (2012) 354-361.
[33] D. Gherca, A. Pui, N. Cornei, A. Cojocariu, V. Nica, O. Caltun, *Synthesis, characterization and magnetic properties of MFe_2O_4 M=Co, Mg, Mn, Ni) nanoparticles using ricin oil as capping agent*, J. Magn. Magn. Mater. 324 (2012) 3906-3911.
[34] **A. Doaga**, A.M. Cojocariu, W. Amin, F. Heib, M. Schmitt, P. Bender, R. Hempelmann, B. Parvatheeswara, O.F. Caltun, *Simple preparation of $Co_xFe_{1-x}Fe_2O_4$ nanoparticles and their potential for hyperthermia applications*, trimis spre publicare la J. Magn. Magn. Mater.
[35] E. Natividad, M. Castro, A. Mediano, Adiabatic vs. non-addiabatic determination of specific absorption rate of ferofluids, J. Magn. Magn. Mater. 321 (2009) 1497 – 1500.
[36] J. Giri, P. Pradhan, T. Sriharsha, D. Bahadur, J. Appl. Phys. 97 (2005) 10Q196 1-10Q196 3.
[37] R.F. Penoyer, M.W. Shafer, J. Appl. Phys 30 (1959) 315S
[38] **A. Doaga**, A.M. Cojocariu, C.P. Constantin, R. Hempelmann, O.F. Caltun, Magnetic nanoparticles for medical applications: progress and challenges, acceptat spre publicare la AIP Proceed.

ANNEX 2
List of ISI publications

1. A. Cojocariu, **A. Doagă**, W. Amin, P. Bender; R. Hempelmann, O.F. Călțun, „*Synthesis and functionalization of magnetic nanoparticles with possible application in drug delivery systems*", Digest Journal of Nanomaterials and Biostructures, Vol. 8, Nr 2 (2013) pag. 519 -527 (Factor de impact 1.2).
2. **A. Doagă**, A.M. Cojocariu, W. Amin, F. Heib, R. Hempelmann, O.F. Călțun, *Synthesis and characterization of manganese ferrites for hyperthermia applications*, trimis spre publicare Materials Chemistry and Physics.
3. **A. Doagă**, A.M. Cojocariu, C.P. Constantin, R. Hempelmann, O.F. Călțun, *Magnetic nanopartices for medical applications: progress and challanges*, accepted for publication in AIP Proceed.
4. **A. Doagă**, A.M. Cojocariu, W. Amin, F. Heib, M. Schmitt, P. Bender, R. Hempelmann, B. Parvatheeswara Rao, O.F. Călțun, *Simple preparation of CoxFe1-xFe2O4 nanoparticles and their potential for hyperthermia applications*, trimis spre publicare Journal of Magnetism and Magnetic Materials.

List of non-ISI publications

1. C.P. Constantin, **A. Doagă**, A.M. Cojocariu, I. Dumitru, O.F. Călțun, *Improved contrast agents for magnetic nuclear resonance medical imaging*, Journal of Advanced Research in Physics, Vol 2, Nr. 1 (2011) pag. 011106- 1-4.
2. **A. Doagă**, C. Constantin, A. Cojocariu, I. Aştefănoaei, I. Dumitru, O. F. Călțun, *Phenomenological study of the thermal field generated by nanoparticles arrays in hyperthermia as treatment method*, Journal of Advanced Research in Physics, Vol 2, Nr. 1 (2011) pag. 011110 -1-4.

ANNEX 3
List of participations in international conferences

- Oral presentations: 5
- Poster presentations: 15

List of participations in national conferences

- Poster presentations: 3